

Anisotropy and oxygen-stoichiometry dependence of the dielectric tensor of $\text{YBa}_2\text{Cu}_3\text{O}_{7-\delta}$ ($0 \leq \delta \leq 1$)

J. Kircher, M. K. Kelly, S. Rashkeev, M. Alouani, D. Fuchs, and M. Cardona

Max-Planck-Institut für Festkörperforschung, Heisenbergstrasse 1, D-7000 Stuttgart 80, Federal Republic of Germany

(Received 26 October 1990)

The dielectric tensor elements of oriented $\text{YBa}_2\text{Cu}_3\text{O}_{7-\delta}$ samples, as obtained by spectroscopic ellipsometry, are presented for several oxygen stoichiometries in the photon energy range between 1.66 and 5.5 eV. For $\delta=0$ and 1, we extend this range up to 9.5 eV using a recently developed synchrotron radiation ellipsometer. We compare the experimental results with computed values for the dielectric function obtained from a linear-muffin-tin-orbitals band-structure calculation. We find good general agreement for both the orientational and compositional dependence. In particular, both experiment and theory show c polarization for a peak near 2.7 eV for $\delta < 0.5$, while a transition in that spectral region is a polarized for $\text{YBa}_2\text{Cu}_3\text{O}_6$. In spite of the difficulty in predicting insulating behavior of the low-oxygen material, these results show that the local-density-approximation picture is successful in describing much of the electronic structure determining higher-energy excitations. In addition, the measured dependence of the dielectric tensor on the oxygen stoichiometry provides a reference for optical determination of the oxygen content and orientation in applications, such as thin-film or single-crystal growth.

I. INTRODUCTION

The discussion about the correct model for the description of the electronic structure of the high- T_c superconductors is still a lively one and far from being decided. The correct description should allow one to calculate both the density of states (as experimentally determined by photoemission and inverse photoemission) and the joint density of states (as determined by various methods of measuring the dielectric function). Since these materials are either orthorhombic (as $\text{YBa}_2\text{Cu}_3\text{O}_7$) or tetragonal (as $\text{YBa}_2\text{Cu}_3\text{O}_6$), the dielectric function is a tensor rather than a scalar. Thus all tensor components have to be compared separately with the results of a calculation in order to determine its validity. In this work we present oxygen-stoichiometry dependent data of the dielectric tensor components parallel and perpendicular to the c axis. We compare these results to optical properties computed from LMTO band-structure calculations for $\text{YBa}_2\text{Cu}_3\text{O}_6$ and $\text{YBa}_2\text{Cu}_3\text{O}_7$.

Earlier studies of the dielectric function of $\text{YBa}_2\text{Cu}_3\text{O}_{7-\delta}$ showed interesting dependence on oxygen stoichiometry^{1,2} as well as on temperature.³ These measurements were performed on randomly oriented multigrained samples. Accurate comparison to band-structure calculations however, requires separation of the dielectric tensor elements. Experimental data of the a - c -anisotropy of $\text{YBa}_2\text{Cu}_3\text{O}_6$ as obtained by ellipsometry⁴ and reflectance⁵ on oriented samples provided results that have been compared with calculations of the dielectric function from a band structure obtained by the LMTO method.⁴ This has contributed to the assignment of a peak at 4.1 eV whose origin had been subject to some controversy.^{1,2,6} The anisotropy of the superconducting $\text{YBa}_2\text{Cu}_3\text{O}_{7-\delta}$ is a more complex subject, since this material is biaxial. The reflectance along the a and b axes

has been directly measured on an untwinned portion of a single crystal surface.^{7,8} Most of this work¹⁻⁷ has been focused on a few prominent features in the optical spectra up to 6 eV.

In this paper we extend the anisotropy studies to the full range of oxygen stoichiometries. For the $\delta=0.15$ and $\delta=0.9$ materials we also extend the anisotropic measurements up to an energy of 9.5 eV and give a comparison with theoretical results. We find good general agreement between experiment and theory. In particular, an absorption feature at 2.7 eV in the spectra for high-oxygen material shows strong c polarization, while a feature at a similar energy for low-oxygen content is a polarized. This behavior is also obtained from the calculated electronic structure (for $\delta=1$). Further agreement is also seen at higher energies. The measurements at intermediate oxygen content, where calculations should be complicated by oxygen disorder, provide insight into the evolution of the electronic structure between the two extremes. In addition to the value of these measurements for modeling the electronic structure, they provide a standard for systematic characterization of oxygen content and orientation by optical techniques. Such techniques are especially valuable in cases where a nondestructive and simple method is needed.

II. EXPERIMENT

The nature of the samples is particularly important to these experiments, since relatively large surfaces containing the c axis are needed. For the optical measurements, crystals were grown using the K_2CO_3 flux method⁹ by heating a mixture of Y_2O_3 , BaCO_3 , K_2CO_3 , and CuO in the molar ratio (0.5):(1.8-2.0):(0.1-0.5):(3.0) at 1270 K for 40 h in a recrystallized alumina crucible, followed by slow cooling. The lower part of the reacted charge is a

porous mixture of polycrystalline $\text{YBa}_2\text{Cu}_3\text{O}_{7-\delta}$ contaminated with Al, K, and other phases like BaCuO_2 , CuO , and Y_2CuBaO_5 (the “green phase”), while the upper portion contains many crystals grown adjacent to each other (with up to five neighboring grown crystals having the same orientation). Each of these crystals consists of several layers ($d=20\text{--}100\ \mu\text{m}$) of single crystals of $\text{YBa}_2\text{Cu}_3\text{O}_{7-\delta}$ with the c axes approximately aligned. Deviations from the average c direction were less than 5° [estimated by scanning electron microscopy (SEM) microstructure analysis] while the directions of the a and b axes were not determined exactly and might vary between different layers. SEM investigations on free-standing crystals, however, indicate that the a and b axes are also largely oriented along either one of two perpendicular directions. The superconducting transition temperature of this material (after oxygen annealing at 820 K for 48 h and subsequent cooling) was found to be 90 K with a transition width of 2 K (as obtained by resistivity measurements). From the upper portion of the material so obtained, samples large enough for optical experiments were cut (typical size $4\times 4\times 4\ \text{mm}^3$). The cutting planes were chosen in a way such that the c axis lay in one of the surfaces of the sample.

These samples were first annealed in oxygen atmosphere at 980 K for 13 h and then cooled slowly to obtain homogeneous samples with the stoichiometry $\text{YBa}_2\text{Cu}_3\text{O}_7$. This procedure was followed by a second annealing process in vacuum with subsequent quenching in order to achieve various oxygen stoichiometries. During this second annealing process the weight loss of the samples was monitored to determine the oxygen stoichiometry. For the kinetics of this annealing process it was found that the samples behave like ceramics rather than single crystals grown by other methods. This may be understood by noting that the method as described above does not yield huge single crystals but rather a very thick stack of thin single-crystal platelets whose c axes are all aligned and that are separated by voids and less dense material.⁹ Probably due to this porous structure of the material the oxygen seems to diffuse rather quickly. Raman spectroscopy¹⁰ was subsequently used to cross-check the oxygen content with an accuracy of $\Delta x = 0.1$.¹¹

Although ellipsometry is a self-normalizing method and therefore rather insensitive to scattering from macroscopic roughness and surface pits, the sample surface containing the c axis was polished to achieve a bigger portion of the surface reflecting into the detector and, by these means, a more favorable signal-to-noise ratio. Polishing was done by first grinding the samples on 800-grit and 4000-grit papers and a final polish by using $0.025\text{-}\mu\text{m}$ methanol-soluble diamond paste on silk. Because the polishing was performed after the vacuum annealing step we avoid any possible surface compositional inhomogeneity due to the annealing.

The pseudodielectric function of these samples, assuming an isotropic two-phase model, was determined by rotating analyzer ellipsometry.¹² Two different instruments were used for these measurements. A conventional spectroscopic ellipsometer was used for the measurements up to approximately 5.5 eV.¹³ All optical components are in

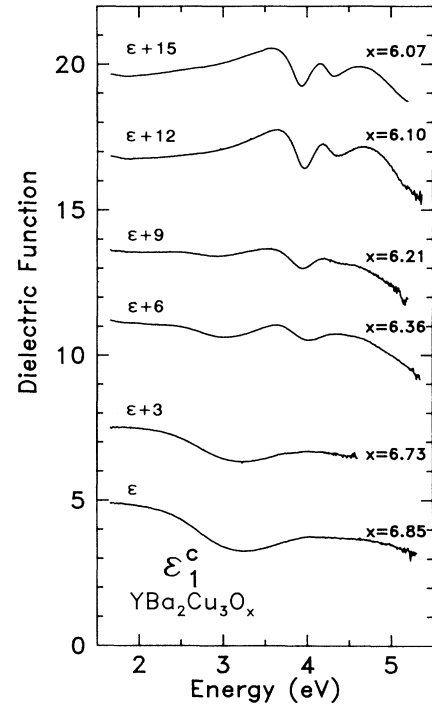


FIG. 1. Real part of the dielectric tensor component along the c axis of $\text{YBa}_2\text{Cu}_3\text{O}_{7-\delta}$ for different oxygen stoichiometries. The curves are shifted vertically by 3 units with respect to each other.

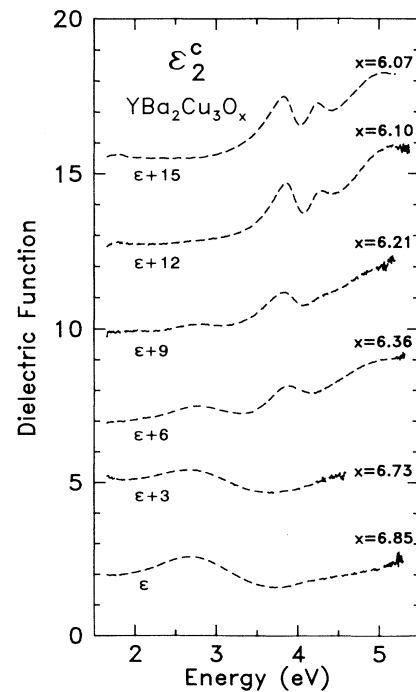


FIG. 2. Imaginary part of the dielectric tensor component along the c axis of $\text{YBa}_2\text{Cu}_3\text{O}_{7-\delta}$ for different oxygen stoichiometries. The curves are shifted vertically by 3 units with respect to each other.

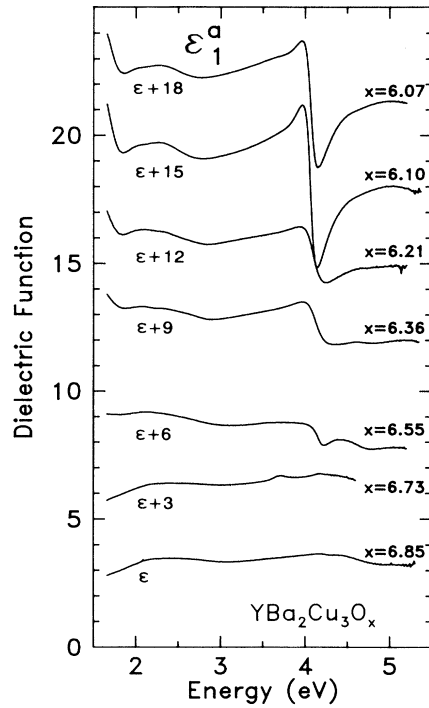


FIG. 3. Real part of the dielectric tensor component along the (a,b) axes of $\text{YBa}_2\text{Cu}_3\text{O}_{7-\delta}$ for different oxygen stoichiometries. The curves are shifted vertically by 3 units with respect to each other.

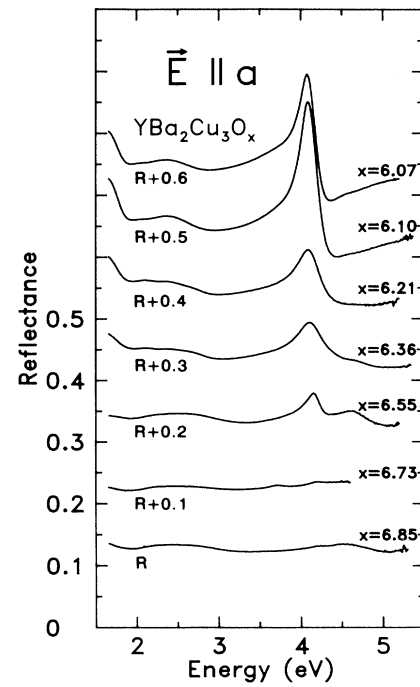


FIG. 5. Reflectance spectra for $\vec{E} \parallel a$ calculated from the ellipsometric data. The spectra are shifted vertically by 0.1 with respect to each other.

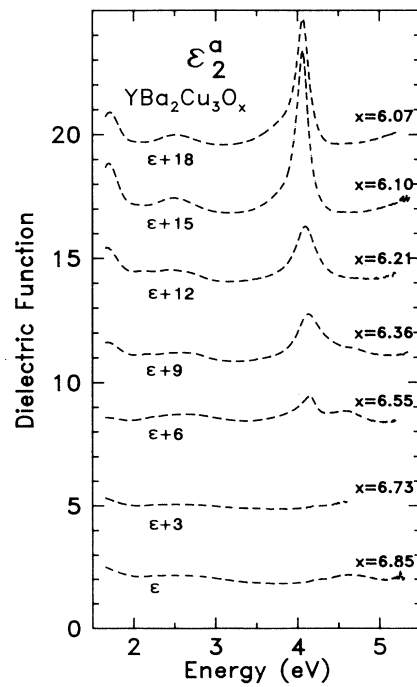


FIG. 4. Imaginary part of the dielectric tensor component along the (a,b) axes of $\text{YBa}_2\text{Cu}_3\text{O}_{7-\delta}$ for different oxygen stoichiometries. The curves are shifted vertically by 3 units with respect to each other.

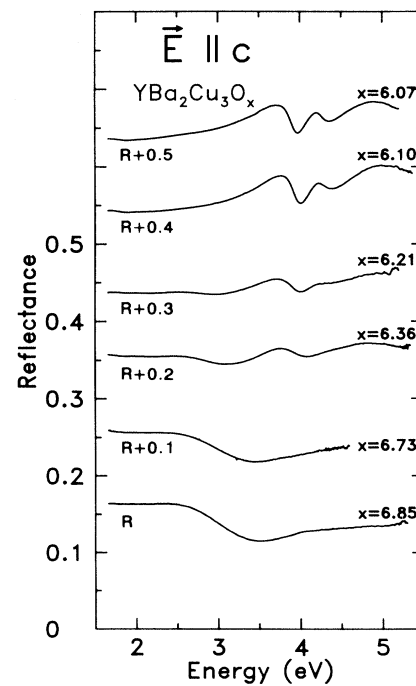


FIG. 6. Reflectance spectra for $\vec{E} \parallel c$ calculated from the ellipsometric data. The spectra are shifted vertically by 0.1 with respect to each other.

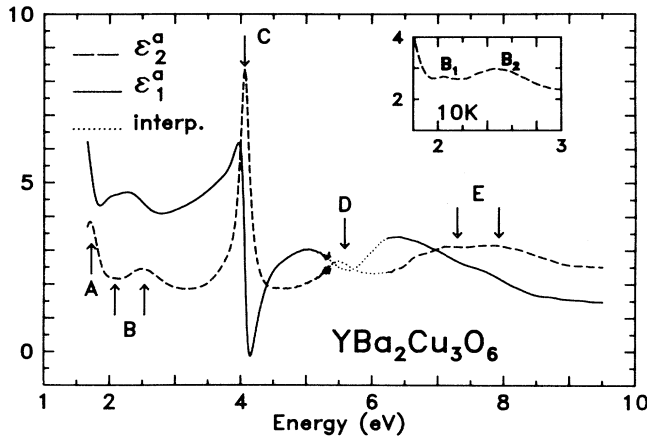


FIG. 7. Extended spectrum of ϵ^a for $\text{YBa}_2\text{Cu}_3\text{O}_6$ including the region in the vacuum uv measured with a synchrotron radiation ellipsometer. The dotted lines indicate an interpolation between the two ellipsometric spectra with the help of reflectance measurements.

air: the sample is either in air or in a cryostat (for the low-temperature measurements). For the high-energy measurements a vacuum ultraviolet (VUV) ellipsometer using synchrotron radiation from the BESSY storage ring was used.¹⁴ Although, in principle, measurements between 6 and 35 eV are possible, poor reflectivity of the samples prevented ellipsometric measurements above 10 eV. We have, however, also measured the reflectance between 4 and 25 eV (Ref. 15) and used these data for interpolation in the energy range between 5 and 6 eV where neither ellipsometer was able to produce reliable data. From the measurement of the pseudodielectric function along two high-symmetry positions, namely c parallel and perpendicular to the plane of incidence, the principal axis components of the dielectric tensor were extracted nu-

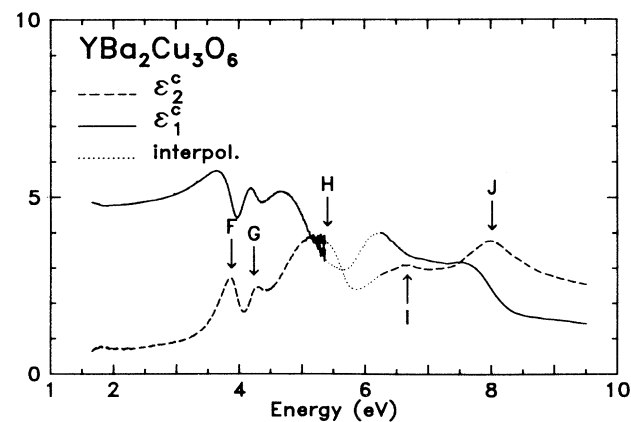


FIG. 8. Extended spectrum of ϵ^c for $\text{YBa}_2\text{Cu}_3\text{O}_6$ including the region in the vacuum uv measured with a synchrotron radiation ellipsometer. The dotted lines indicate an interpolation between the two ellipsometric spectra with the help of reflectance measurements.

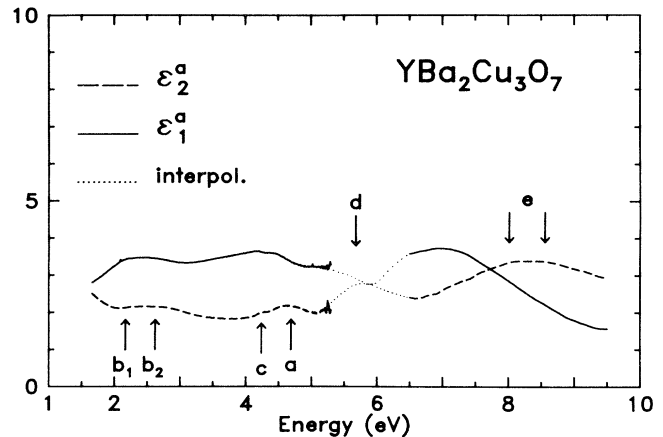


FIG. 9. Extended spectrum of ϵ^a for $\text{YBa}_2\text{Cu}_3\text{O}_7$ including the region in the vacuum uv measured with a synchrotron radiation ellipsometer. The dotted lines indicate an interpolation between the two ellipsometric spectra with the help of reflectance measurements.

merically.^{16,17} Since the a - b -planes were heavily twinned we used a uniaxial model, which is strictly correct for the lower oxygen stoichiometries only. For ease of the subsequent discussion, however, the in-plane components of the experimentally determined dielectric tensor are called ϵ^a in spite of the fact that they really are a mixture of ϵ^a and ϵ^b .

The spectra of the dielectric tensor components for various oxygen stoichiometries are displayed in Figs. 1-4. For comparison with other work, the reflectance spectra were calculated from the experimentally determined dielectric functions. These results are displayed in Figs. 5 and 6. In all these figures the labeling of the y axis shows the correct numerical values for $\text{YBa}_2\text{Cu}_3\text{O}_{6.85}$. Spectra for higher δ are shifted up as indicated in the

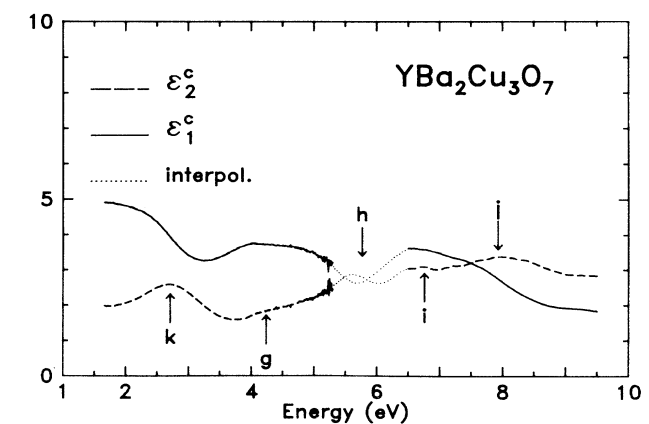


FIG. 10. Extended spectrum of ϵ^c for $\text{YBa}_2\text{Cu}_3\text{O}_7$ including the region in the vacuum uv measured with a synchrotron radiation ellipsometer. The dotted lines indicate an interpolation between the two ellipsometric spectra with the help of reflectance measurements.

figure captions. Figures 7–10 give spectra of the dielectric tensor components of $\text{YBa}_2\text{Cu}_3\text{O}_{6.1}$ and $\text{YBa}_2\text{Cu}_3\text{O}_{6.85}$ in the extended range between 1.66 and 9.5 eV. No adjustable parameters were used to match the high- and low-energy parts of the curve taken with the different instruments. The dotted lines show the interpolation that has been made with the help of reflectance measurements and we should caution that differences in the systematic errors of the two instruments used for the measurements may affect the interpolation. An insert in Fig. 7 shows results of measurements between 1.8 and 3 eV at 10 K. Other spectral regions did not change substantially with temperature. For easier comparison between theory and experiment as well as the subsequent discussion, the peaks in Figs. 7–10 are labeled A, B, C, \dots for the nonsuperconducting ($\delta=1$) compound and a, b, c, \dots for the superconducting ($\delta=0$) compound.

III. THEORY

The experimental results so obtained were compared to theoretical curves for ϵ_2 . Unfortunately, the calculation of $\epsilon(\omega)$ for arbitrary oxygen stoichiometries including oxygen disorder is not feasible for the moment. Thus, instead of following through the evolution of the peaks we can present only the results of calculations for the extreme values of δ ($\delta=0$ or $\delta=1$). For the dielectric function of the insulating compound the electronic states were calculated using the linear-muffin-tin-orbitals method in the atomic sphere approximation¹⁸ with spd orbitals on the oxygens and $spdf$ orbitals on all other atoms. The Brillouin-zone (BZ) integrations were performed using the tetrahedron method with 147 points in the irreducible BZ. Since the procedure used was a one-panel calculation, only data below 6.5 eV are displayed. More details of the calculation and its comparison with experiments are given in Ref. 4 and references therein. The calculated interband ϵ^a and ϵ^c are smoothed by assuming a constant lifetime broadening of 0.1 eV and

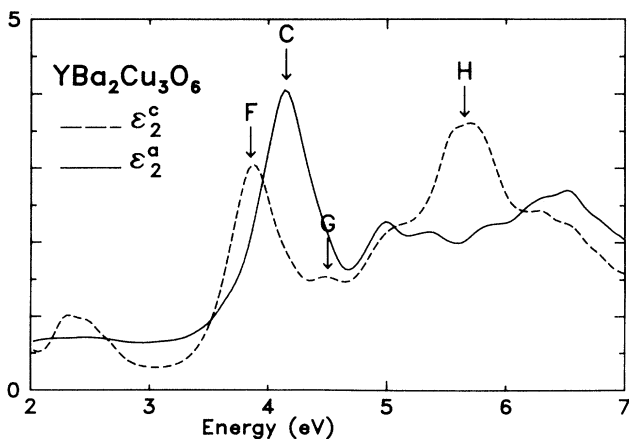


FIG. 11. Theoretical curves for ϵ_2^c and ϵ_2^a for $\text{YBa}_2\text{Cu}_3\text{O}_6$. Both curves are shifted up in energy by 0.5 eV. Note the different energy scale.

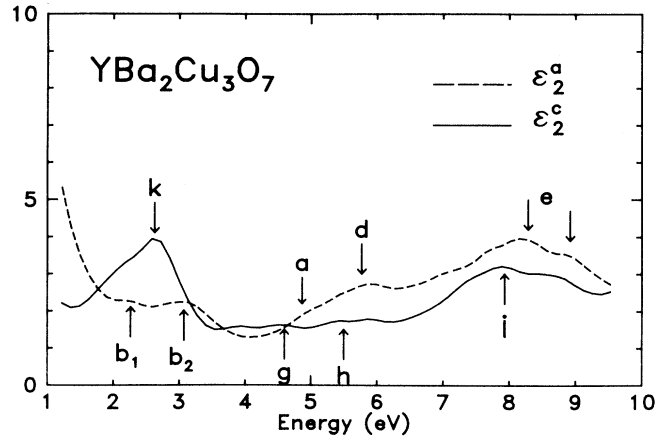


FIG. 12. Theoretical curves for ϵ_2^c and ϵ_2^a for $\text{YBa}_2\text{Cu}_3\text{O}_7$.

shifted up rigidly in energy by 0.5 eV. The resulting curves are shown in Fig. 11.

For the superconducting material with $\delta=0$ the electronic states were also calculated with the LMTO method with the same basis set as above. 242 points in $\frac{1}{8}$ of the BZ were used. From these bands the interband contribution to ϵ_2 was evaluated. For the intraband contribution the Drude model was used. Due to the orthorhombic structure of the material ϵ^a , ϵ^b , and ϵ^c are all different. For the simulation of the experiments an average of ϵ^a and ϵ^b with equal weights was calculated. This mixture is labeled ϵ^a . Both ϵ^a and ϵ^c were smoothed by insertion of a phenomenological lifetime broadening $\gamma=0.15$ eV and are displayed together in Fig. 12. Again for easier discussion and comparison with the experiment the peaks are labeled a, b, c, \dots . More details about this calculation are found elsewhere.¹⁹

IV. DISCUSSION

Figures 1–4 show the changes of the different components of the dielectric tensor with oxygen stoichiometry. The dependence of spectral features on oxygen stoichiometry, as presented here, is compatible with similar data obtained from measurements on polycrystalline samples. At first glance, all the structure in ϵ_2^a weakens with increasing oxygen content, with the exception of one peak at 4.7 eV that is strongest for intermediate ($x=6.55$) and absent for low oxygen stoichiometry. For the c direction, the structures that are characteristic of the insulating compound vanish, but at the same time a new broad structure between 2 and 3 eV builds up. Clearly, in addition to providing electronic structural information (as discussed below), these spectra show features that are unique at any oxygen stoichiometry and orientation and this encourages the use of optical measurements for material and film characterization.²⁰ Although in principle displaying less information, reflectance spectra are often more easily obtained for such purposes, and are therefore included in Figs. 5 and 6. From these it can be seen, however, that reflectance

spectra still contain enough information for characterization purposes. Measuring absolute values of the reflectance at one fixed photon energy (even on the 4.1-eV peak) will most probably be inadequate and also impossible to perform with satisfactory accuracy during film growth. However, the shape of the complete curve (e.g., the ratio of the heights of different peaks and their broadenings) gives unambiguous information about the orientation of the sample and even this qualitative analysis should allow one to determine the oxygen content δ to an accuracy of 0.15. As a recent application of these results for the optical characterization of (110)-oriented $\text{YBa}_2\text{Cu}_3\text{O}_7$ films suggests,²¹ optical measurements of the a - c -anisotropy, which is large for all oxygen contents, can be an especially valuable tool for *in situ* control of the growth of a -axis oriented films, in which recently some progress has been reported.²² Considering the nondestructiveness of the method and the simplicity of the experimental setup for a reflectance measurement, this could be very useful. Note that the penetration depth for these measurements is approximately 500 Å and that the effects of inhomogeneity within this layer would have to be modeled.

We now discuss in detail the various features and compare them with band-structure calculations. The features are labeled A, B, \dots, a, b, \dots , in Figs. 7–12 according to their energy position, which is the same order as will be used for the discussion. Throughout this section the lowest oxygen content sample will be called $\text{YBa}_2\text{Cu}_3\text{O}_6$ and the highest $\text{YBa}_2\text{Cu}_3\text{O}_7$, and the mixture of a and b polarization is referred to simply as a polarization. Comparing the experimentally determined dielectric function for $\text{YBa}_2\text{Cu}_3\text{O}_7$ (Figs. 9 and 10) with the calculated one (Fig. 12) and an earlier theoretical result,²³ we find good agreement for both a and c polarizations. All features are reproduced by the calculation and a detailed analysis of the calculated results should therefore be helpful in assigning the structure in the dielectric function. The situation is different for the insulating compound. Experimental (Figs. 7 and 8) and theoretical (Fig. 11) values do not show the same level of agreement. This can be rationalized by noting that the LDA bands have no gap. These electronic bands close to the Fermi level are responsible for the structures observed below 3 eV. It is this gap problem that probably also causes higher interband transitions to lie at too low energies. For easier comparison with the experiment, the theoretical curves in Fig. 12 are shifted up in energy by 0.5 eV. At higher energies, however, the calculation correctly reproduces the polarization dependence of the dielectric function and in this range the calculation may help with the interpretation of the data. Following is a discussion of the features in order of energy.

The peak at 1.7 (eV) (A) is a polarized and becomes weaker as the metallic character of the material increases with oxygen content. Since the band-structure calculation for the insulating compound fails to reproduce the experimental gap, it does not contribute to the determination of the nature of this peak. Investigation of the anisotropy of the feature revealed no information beyond previous work.^{1,4,6}

Between 2 and 3 eV the optical spectra show detail beyond that previously discussed. Most noteworthy is the buildup of a c -polarized peak (k) around 2.8 eV for the oxygen-rich compounds, as predicted by the band-structure calculations. It is absent for the low-oxygen compound; with decreasing δ the feature grows stronger and broader and shifts to a lower energy position (by about 0.1 eV). In the same energy range we find along the a direction a very small peak at 2.1 eV (B_1) that has received little attention before. It seems to persist for all different oxygen contents, although in some cases it can only be seen weakly in ϵ_1^2 (for small δ) or in low temperature measurements (see insert in Fig. 7). Between 2.5 and 3 eV we find another a -polarized structure (B_2) that also persists for all δ . In the second derivative spectra, this feature seems more complex, showing two small peaks that are hard to separate especially for high oxygen stoichiometries at room temperature. One structure at 2.5 eV is dominating at high δ , a second structure dominating at low δ can be seen at 2.75 eV.

For the same reasons that peak (A) could not be explained by the band-structure calculations we cannot assign the (B) features of the low oxygen samples with the help of these calculations. For the superconducting compound, on the other hand, the situation is different. The calculation not only shows the c -polarized strong feature, but also the broader and weaker a -polarized feature which exhibits some fine structure. Similar behavior was also predicted by an earlier calculation.²³ From the calculation, we conclude that the c -polarized (k) peak originates from transitions into the antibonding $\text{Cu}(1)\text{-O}(1)\text{-O}(4)$ band. [The convention used in this work for labeling of crystallographic sites is that in most common use: $\text{Cu}(1)$ and $\text{O}(1)$ denote copper and oxygen atoms in the chains, $\text{O}(4)$ is the bridging oxygen between the chains and the planes, and $\text{Cu}(2)$, $\text{O}(2)$, and $\text{O}(3)$ are sites in the planes.] The initial state is a band with plane character (approximately 1 eV below the Fermi level) and analysis of the matrix elements show that the largest contributions come from the $\text{Cu}(1)$ and $\text{O}(4)$ spheres, and, to a lesser extent, from the $\text{O}(1)$ spheres. This assignment can also explain why the peak disappears in the nonsuperconducting compound where no chains are present. According to the calculations, a completely different group of transitions is responsible for the weaker structure (b_2) with a orientation. The initial states can be found in the manifold of strongly dispersive bands parallel to the final states which are the antibonding $\text{Cu}(2)\text{-O}(2)\text{-O}(3)$ bands. The assignment of transitions in this energy range to the CuO_2 planes is also consistent with comparisons to other materials with similar structures.⁶

Three features around 4 eV (F, G, C) that are strong for low oxygen content, have previously been assigned to intraionic $\text{Cu}(1)$ transitions,⁴ among them the dominant a -polarized peak at 4.1 eV (C), which is mostly due to a $3d_{3z^2-1} - 4p_x$ excitation within the ion. The assignment to the $\text{Cu}(1)$ site was also obtained based on comparisons with other materials having similar sites.^{2,6} The two other smaller peaks are c polarized (F and G) and caused by $3d_{xx} - 4p_x$ and $3d_{yz} - 4p_y$ transitions. All these peaks

lose intensity and shift to slightly higher energy positions with increasing oxygen content, as can be seen in Figs. 2 and 4. Even at our highest oxygen content, feature (*c*) retains some strength possibly due to residual oxygen vacancies. For the $x = 6.10$ sample (Figs. 3 and 4) the peak is in fact somewhat higher than for the $x = 6.07$ sample. The latter was cut from a different block of material, the Raman measurements for oxygen determination had to be taken on a different spectrometer and the measurements could not be redone together with the other measurements. Nevertheless we included the spectrum to give an indication for the errors from the Raman as well as from the ellipsometric measurements.

Another feature along the *a* axis shows interesting behavior: the peak at 4.8 eV (see Fig. 4) sharpens for intermediate oxygen stoichiometries and is not detectable for O_6 and very broad for O_7 . This feature might be related to the presence or the ordering of the chains in materials with intermediate oxygen stoichiometry. Another argument in favor of this assignment is the experimental finding that this feature is predominantly polarized along the chains.⁷

The experimental behavior of a rather wide absorption feature above 5 eV (peaks *D*, *H*, *d*, *h* in Figs. 7–12) is too uncertain to be discussed on the basis of our data. As it was mentioned above, reflectance data also obtained at the BESSY synchrotron laboratory on the same sample had to be used for interpolation between the low-energy and the high-energy parts of the ellipsometric spectra. All available experimental data including those on a different ellipsometer on ceramic samples, indicate that there is a feature in this region.² However, possible differences in systematic errors between the low- and high-energy machines used for our work do not permit detailed discussion of energy positions and widths of these features. The band-structure calculations also predict features between 5 and 6 eV corresponding to transitions into empty bands with predominantly Ba *d* and Y *d* characters, with admixtures of Ba *f* and Cu *p* orbitals.

A similar origin—with more Cu *p* admixture to the final state—is assigned to the features at higher energies. The most interesting behavior in this energy region, however, is the strong orientational dependence of the peak at

8 eV (*J*, *E*) for the low-oxygen material. The band-structure calculations for the semiconducting materials, as mentioned above, are limited to below 6 eV, and are of no help in this case. The same orientational behavior was found in our reflectance data¹⁵ on samples of the same type. Single-crystal measurements performed by other groups did not yield data for $E_{||c}$.^{14,24} Independent confirmation of this feature is clearly necessary.

V. CONCLUSIONS

We have presented oxygen-stoichiometry dependent and polarization dependent data of the dielectric tensor of $YBa_2Cu_3O_{7-\delta}$ obtained by rotating analyzer ellipsometry. For extreme oxygen stoichiometries the experimental data have been extended to 9.5 eV and compared to theoretical values obtained from an LMTO band-structure calculation. While for the nonsuperconductor the agreement is limited to a rather small energy range due probably to the gap problem in the calculations up to 3 eV and to the lack of calculations above 7 eV, the agreement for the superconductor is good across the whole spectral range under consideration. This indicates that LDA calculations produce reasonable descriptions of the electronic structure of HTC materials in the normal state. We also extend the dielectric tensor data to intermediate oxygen stoichiometries, showing the evolution of the differences in the optical spectra of the superconductor and the nonsuperconductor and establishing a reference for optical material characterization.

ACKNOWLEDGMENTS

We are deeply indebted to C. Thomsen, O. K. Andersen, and E. T. Heyen for many clarifying discussions and to P. Murugaraj for the preparation of the samples. We also wish to thank D. Schönherr for the thermogravimetric measurements, and E. T. Heyen for the Raman measurements. One of us (M.K.K.) would like to acknowledge the support by the Alexander von Humboldt Foundation. The synchrotron radiation ellipsometer is funded by the German Minister of Research (BMFT) under Contract No. 05490CAB.

¹M. Garriga, J. Humlíček, M. Cardona, and E. Schönherr, *Solid State Commun.* **66**, 1231 (1988).

²M. K. Kelly, P. Barboux, J.-M. Tarascon, D. E. Aspnes, W. A. Bonner, and P. A. Morris, *Phys. Rev. B* **38**, 870 (1988).

³M. Garriga, J. Humlíček, J. Barth, and R. L. Johnson, *J. Opt. Soc. Am. B* **6**, 470 (1989).

⁴J. Kircher, M. Alouani, M. Garriga, P. Murugaraj, J. Maier, C. Thomsen, M. Cardona, O. K. Andersen, and O. Jepsen, *Phys. Rev. B* **40**, 7368 (1989).

⁵H. Romberg, N. Nücker, J. Fink, Th. Wolf, X. X. Xi, B. Koch, H. P. Geserich, M. Dürler, W. Assmus, and B. Gegenheimer (unpublished).

⁶M. K. Kelly, P. Barboux, J. M. Tarascon, and D. E. Aspnes, *Phys. Rev. B* **40**, 6797 (1989).

⁷B. Koch, H. P. Geserich, and Th. Wolf, *Solid State Commun.* **71**, 495 (1989).

⁸M. P. Petrov, A. I. Grachev, M. V. Krasin'kova, A. A. Nechitailov, V. V. Prokofiev, V. V. Poborchy, S. I. Shagin, and N. F. Kartenko, *Solid State Commun.* **67**, 1197 (1988).

⁹P. Murugaraj, M. Maier, and A. Rabenau, *Solid State Commun.* **71**, 167 (1989).

¹⁰C. Thomsen, R. Liu, M. Bauer, A. Wittlin, L. Genzel, M. Cardona, E. Schönherr, W. Bauhofer, and W. König, *Solid State Commun.* **65**, 55 (1988).

¹¹B. Friedl (private communication).

¹²D. E. Aspnes and A. A. Studna, *Appl. Opt.* **14**, 220 (1975).

¹³L. Viña, S. Logothetidis, and M. Cardona, *Phys. Rev. B* **30**, 1979 (1984).

- ¹⁴R. L. Johnson, J. Barth, M. Cardona, D. Fuchs, and A. M. Bradshaw, *Rev. Sci. Instrum.* **60**, 2209 (1989).
- ¹⁵J. Kircher (unpublished).
- ¹⁶S. Logothetidis, M. Cardona, P. Lautenschlager, and M. Garriga, *Phys. Rev. B* **34**, 2458 (1986).
- ¹⁷M. Garriga, Ph.D. Thesis, University of Stuttgart, 1990.
- ¹⁸O. K. Andersen, *Phys. Rev. B* **12**, 3060 (1975).
- ¹⁹E. G. Maksimov, S. N. Rashkeev, S. Yu. Savrasov, and Yu. A. Uspenskii, *Phys. Rev. Lett.* **63**, 1880 (1989).
- ²⁰M. K. Kelly, S.-W. Chan, K. Jenkin II, D. E. Aspnes, P. Barboux, and J.-M. Tarascon, *Appl. Phys. Lett.* **53**, 2333 (1988).
- ²¹H.-U. Habermeyer, A. A. C. S. Lourenço, B. Friedl, J. Kircher, and J. Köhler, *Solid State Commun.* **77**, 683 (1991).
- ²²C. B. Eom, A. F. Marshall, S. S. Laderman, R. D. Jacowith, and T. H. Geballe, *Science* (to be published).
- ²³Guang-Lin Zhao, Yongnian Xu, W. Y. Ching, and K. W. Wong, *Phys. Rev. B* **36**, 7203 (1987).
- ²⁴S. Tajima, H. Ishii, T. Nakahashi, H. Takagi, S. Uchida, M. Seki, S. Suga, Y. Hidaka, M. Suzuki, T. Murakami, K. Oka, and H. Unoki, *J. Opt. Soc. Am. B* **6**, 475 (1989).